J. Phys.: Condens. Matter 5 (1993) 4505–4518. Printed in the UK

Local spin clustering and phase separation in the Hubbard model

A N Andriotis, E N Economou and C M Soukoulis†

Research Center of Crete and Department of Physics, University of Crete, PO Box 1527, 71110 Heraklion, Crete, Greece

Received 5 January 1993

Abstract. We use an unrestricted self-consistent mean-field approach to the one-dimensional periodic Hubbard model to study its ground-state phase diagram. Our approach allows one to incorporate spin and electron correlations as well as spin and charge fluctuations. We find that a homogeneous antiferromangetic state exists only at half-filling, where the state is also insulating. Off half-filling, it was found that the ground state of the Hubbard model consists of clusters with different magnetic and charge properties. For certain values of the parameters of the system the cluster formation develops to a full phase separation. The effects of the intersite repulsive or attractive interaction on the ground-state properties were also examined. Implications of our results for the existence of a superconducting ground state as well as comparison with other studies will be briefly discussed.

1. Introduction

One of the main problems in the field of high-T_c superconductivity is the understanding of its microscopic mechanisms. Most of the proposed mechanisms are discussed in the context of theoretical models which employ certain rather drastic approximations. Among these models, the Hubbard [1] model and the related t–J model [2] have received special attention in view of the strong electron–electron correlations in high-T_c superconductors and in related compounds [3]. Nonetheless and despite strong theoretical efforts during the last few years, many fundamental aspects of the solution of the Hubbard model still remain unclear, especially in the case of the two-dimensional (2D) [4–6] and three-dimensional (3D) systems. For these systems the problems of neglecting charge and spin correlations as well as charge and spin fluctuations from the solutions of the Hubbard model become more pronounced in the description of the $T = 0$ phase diagram of the Hubbard model which remains still not clear. Recent work on the t–J model indicated that a phase-separated [7] state is a possible ground state of this model when the parameters are in a certain range. Indications for phase separation were also found by us [8] in the Hubbard model using the correlated random field approximation (CRFA) and the conditional coherent potential approximation (CPA) using a Bethe lattice description of our system for which simple analytic expressions for the Green functions exist [12].

The recent interest in a possible phase separation in the Hubbard model and its implication for the relevance of the latter to the high-T_c superconductivity made us undertake a systematic re-examination of the phase diagram at $T = 0$ including effects due to magnetic and charge correlations.

† Permanent address: Ames Laboratory and Department of Physics, Iowa State University, Ames, IA 50011, USA.

0953-8984/93/264505+14$07.50

In the present work in order to check our results that we obtained within the CRFA and the conditional CPA further and in order to study more carefully the effects of charge and spin correlations and fluctuations on the ground system of the system, we examine the one-dimensional (1D) periodic Hubbard model in an unrestricted self-consistent mean-field approximation (MFA). Our results are compared with corresponding data for the 1D Hubbard model obtained within the Bethe lattice description and the CRFA and the conditional CPA [8, 11, 13]. Both results are shown on a magnetic phase diagram (figure 6 below) and, as will be demonstrated, they are mutually supportive; both model descriptions indicate areas of the phase diagram where the ground state of the system favours phase separation.

Recently, on the basis of the exact solution obtained by Lieb and Wu [14], several workers [15–17] have obtained exact results for the correlation functions in the 1D Hubbard model. According to these results the ground state has zero total magnetic moment with short-range antiferromagnetic (AF) and charge correlations. In spite of the existence of these exact results, our MFA is instructive and meaningful, because it allows us to obtain a more direct physical picture of the many-body correlations, while at the same time it determines the limitations of the MFA under the extreme conditions of the one-dimensionality. This puts the MFA on a firmer basis in two and three dimensions, where no exact results are available. The general tendency of the mean-field theories to be independent of the dimensionality (at the qualitative level) is reinforced in the present case where the results of the CRFA for the 3D Hubbard model are qualitatively similar to the results of the MFA in the 1D case.

2. Formalism

We have employed the one-band Hubbard Hamiltonian

$$H = \sum_{i\sigma} \epsilon_0 n_{i\sigma} + \sum_{i,j,\sigma i\neq j} V_{ij}\alpha^+_{i\sigma}\alpha_{j\sigma} + U\sum_i n_{i\sigma}n_{i-\sigma} + U_1\sum_i n_i(n_{i-1}+n_{i+1}) \tag{1}$$

where the sites (i) form a periodic lattice, σ is taken to be +1 for spin up and −1 for spin down; ϵ_0 is a constant which can be taken as zero, V_{ij} is the transfer integral which is taken to be a constant V when i, j are nearest neighbours and zero otherwise, U is the on-site Coulomb repulsion and $n_{i\sigma} = \alpha^+_{i\sigma}\alpha_{i\sigma}$ with $\alpha^+_{i\sigma}, \alpha_{i\sigma}$ being the creation and annihilation operators, respectively. Finally, U_1 describes the intersite Coulomb interactions which in our case is limited to only nearest neighbours. The physical parameters of the model are

(i) the ratios U/V and U_1/V,
(ii) the average number n of electrons per lattice site and
(iii) the type of lattice.

Owing to particle–hole symmetry, one obtains identical results for n and $2-n$. Thus we can restrict ourselves to the range $0 \leqslant n \leqslant 1$.

Our approximation is based on Hubbard's original suggestion according to which the cumbersome many-body U-term of equation (1) is replaced by a random one-body term, i.e.

$$Un_{i\sigma}n_{i-\sigma} \simeq \epsilon_{i\sigma}n_{i\sigma} \tag{2}$$

where $\epsilon_{i\sigma}$ are correlated random variables, the distribution of which is determined self-consistently. With this approximation, equation (1) is decoupled to one-spin Hamiltonians

$$H_\sigma = \sum_i \epsilon_{i\sigma}|i\sigma\rangle\langle i\sigma| + V\sum_{i\neq j}|i\sigma\rangle\langle j\sigma| \tag{3}$$

where

$$\epsilon_{i\sigma} = \epsilon_0 + U\langle n_{i-\sigma}\rangle + U_1(\langle n_{i-1}\rangle + \langle n_{i+1}\rangle). \tag{4}$$

Our self-consistent MFA to the 1D periodic Hubbard system can include both charge and spin fluctuations and correlations by allowing the system to evolve from an arbitrary set of initial input parameters towards a self-consistent solution. We employ an (approximate) periodic supercell arrangement and choose the number n of electrons per lattice site in such a way as to allow a number M of electrons to be distributed over the N sites of the unit supercell ($M/N = n < 1$). When M is chosen to be an integer, it is noted that such an artificially imposed periodicity with an integer M favours a Peierls instability and a lowering of the total energy. We have also relaxed this restriction of integer M on n without any qualitative change. Within each unit supercell the spin and charge fluctuations are unrestricted and are determined self-consistently with our MFA described by equations (2)–(4).

The solution of the Hamiltonian H_σ will provide the electron numbers $\langle n_{i\sigma}\rangle$, $i = 1, \ldots, N$, for the N sites of the unit supercell, in terms of a given set of electron numbers $\langle n_{i-\sigma}\rangle$ of the opposite spin $-\sigma$. The calculated electron numbers $\langle n_{i\sigma}\rangle$ are subsequently used to solve $H_{-\sigma}$ (given by equations (3) and (4)) by replacing σ by $-\sigma$ from which a new set of $\langle n_{i-\sigma}\rangle$ is obtained. This set is used as input to equation (3) and H_σ is solved again to obtain the new $\langle n_{i\sigma}\rangle$. The whole procedure is repeated until self-consistency with respect to the sets $\langle n_{i\pm\sigma}\rangle$ is achieved. This self-consistency is equivalent to an extremum of the total energy of the system. In the case of multiple solutions the one with the lower total energy is chosen.

Our calculational procedure employs the periodicity of the supercell structure to solve

$$H_\sigma|k\nu\sigma\rangle = E_{k\nu\sigma}|k\nu\sigma\rangle \tag{5}$$

by expanding $|k\nu\sigma\rangle$ as

$$|k\nu\sigma\rangle = \frac{1}{\sqrt{N}}\sum_{i=1}^{N} c_{i\nu\sigma}|i\sigma\rangle \tag{6}$$

where ν denotes the band index. Using Bloch's theorem ($c_{j+N,\nu\sigma} = c_{j\nu\sigma}\exp(ikNd)$, where d is the lattice constant), and substituting equation (6) into (5) we obtain the following $(N \times N)$ matrix equation:

$$(H_\sigma - E_{k\nu\sigma})y_{k\nu\sigma} = \mathbf{0} \tag{7}$$

where the matrix elements $H_{ij\sigma}$ of H_σ are

$$H_{ij\sigma} = \epsilon_{i\sigma}\delta_{ij} + \sum_{i\neq j} V_{ij}\exp[ik(r_i - r_j)] \tag{8}$$

and the components $y^{(i)}_{k\nu\sigma}$ of the solution vector $y_{k\nu\sigma}$ are the expansion constants $c_{i\nu\sigma}$.

The diagonalization of $H_{ij\sigma}$ is performed for various k-points belonging to the first Brillouin zone of the lattice. The number of k-points (which in our case is 300) is specified by the required accuracy in the k-integrations which are necessary for obtaining the $\langle n_{i\pm\sigma}\rangle$. In particular, for each k-vector we calculate the Green function

$$G_{k\nu\sigma}(E) = \sum_{i=1}^{N} \frac{y^{(i)*}_{k\nu\sigma} y^{(i)}_{k\nu\sigma}}{E - E^{(i)}_{k\nu\sigma}}. \tag{9}$$

Having obtained $G_{k\nu\sigma}(E)$ we can find the electron density of states (DOS), denoted by $\varrho_\sigma(E)$:

$$\varrho_\sigma(E) = -\frac{1}{\pi}\mathrm{Im}\left(\sum_{k\nu} G_{k\nu\sigma}(E)\right). \tag{10}$$

The maximum number of occupied electron bands and the Fermi energy E_F of the system is specified from the condition

$$\sum_\sigma \int_{-\infty}^{E_F} \varrho_\sigma(E)\,\mathrm{d}E = nN \tag{11}$$

which is imposed by the given average number n of electrons per lattice site. Finally,

$$\langle n_{i\sigma}\rangle = -\frac{1}{\pi}\sum_{k\nu}\mathrm{Im}\left(\int_{-\alpha}^{E_F} \frac{y_{k\nu\sigma}^{(i)*} y_{k\nu\sigma}^{(i)}}{E - E_{k\nu\sigma}^{(i)}}\,\mathrm{d}E\right). \tag{12}$$

The magnetic moment μ_i per lattice site and the electron density n_i per lattice site can be obtained from the expressions

$$\mu_i = \langle n_{i\sigma}\rangle - \langle n_{i-\sigma}\rangle \qquad i = 1, \ldots, N \tag{13}$$

$$n_i = \langle n_{i\sigma}\rangle + \langle n_{i-\sigma}\rangle \qquad i = 1, \ldots, N \tag{14}$$

while the energy of the system per lattice site is obtained from the expression

$$E = \frac{1}{N}\sum_{k,\nu,\sigma_{\text{occupied}}} E_{k\nu\sigma} - \frac{1}{N}\sum_{i=1}^{N} U\langle n_{i\sigma}\rangle\langle n_{i-\sigma}\rangle - \frac{1}{N}\sum_{i=1}^{N} U_1 n_i(n_{i-1} + n_{i-1}) \tag{15}$$

assuming that $\epsilon_0 = 0$.

3. The ground state for the 1D periodic lattice

The main qualitative features of our results for the 1D periodic lattice are indicated in figure 1 where we show the configuration of the lowest-energy state of a system with $N = 6$ and $n = \frac{5}{6}$ for $U_1 = 0$ and various values of U/B (B being the half-band width, i.e. $B = 2V$ for the 1D case). On the left of the figure we show the magnetic moments μ_i, $i = 1, \ldots, N$ and on the right we show the number n_i of electrons per lattice site as calculated according to equations (13) and (14). For not so high values of U/B we have found that the lowest-energy configuration exhibits a tendency to develop clusters of ferromagnetic (F) and AF order within the unit cell as shown in figure 1. This type of state that exhibits such clustering features is named a cluster state (C state). As U/B increases, the C state with the lowest energy still exhibits F–AF clustering but now the F cluster has grown larger at the expense of the AF cluster. For much larger U/B-values the lowest-energy state of the system exhibits F order all over the unit cell. It must be pointed out that the MFA tends to overestimate the

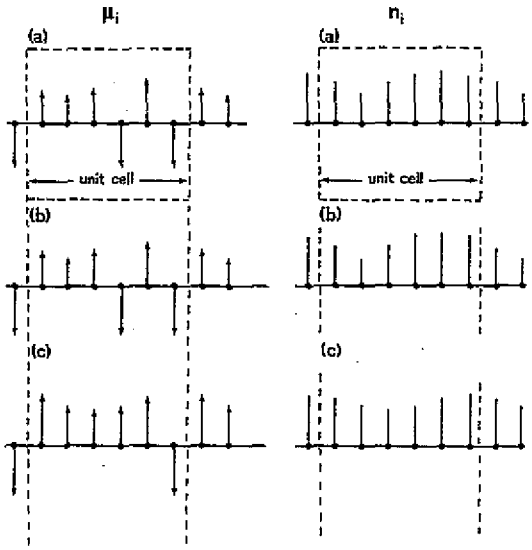

Figure 1. The ground-state values for the magnetic moments μ_i (left-hand side) and the electron numbers n_i (right-hand side) at each site i of the unit cell (confined between the vertical dashed lines) of a 1D periodic Hubbard system with $N = 6$, $n = \frac{5}{6}$, $U_1 = 0$ and various values of U/B: (*a*) $U/B = 2.5$; (*b*) $U/B = 4.0$; (*c*) $U/B = 7.5$.

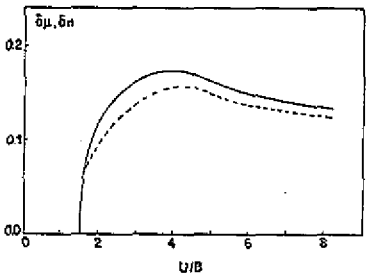

Figure 2. Variation with U/B in the deviations δn (——) and $\delta\mu$ (– – –) defined according to equations (24) and (25), respectively, for a 1D periodic Hubbard system with $N = 6$, $n = \frac{5}{6}$ and $U_1 = 0$.

F correlations compared with the exact results which do not produce even medium-range F order.

In figure 1 it is also observed that the number of electrons per lattice site exhibits a substantial fluctuation (charge fluctuation) from site to site. A quantitative picture of this fluctuation can be obtained by calculating the deviation δn of the number n_i of electrons relative to its mean value:

$$\delta n = \sqrt{\frac{1}{N}\sum_{i=1}^{N}(n_i - n)^2}. \tag{16}$$

A similar expression for the deviation $\delta\mu$ for the magnetic moments is obtained from the formula

$$\delta\mu = \sqrt{\frac{1}{N}\sum_{i=1}^{N}(|\mu_i| - |\mu|)^2} \tag{17}$$

where $|\mu|$ is the average absolute value of the μ_i.

In figure 2 we show the variation in δn and $\delta\mu$ as U/B varies for a system of $N = 6$, $n = \frac{5}{6}$ and $U_1 = 0$. It is observed that both δn and $\delta\mu$ exhibit a maximum as U/B increases and then they drop off slowly and become zero at very large U/B where the system attains the F state. It is worth noting that the charge fluctuations shown in figure 1 are distributed in such a way within the unit cell that the excess charge is associated with the AF cluster while the lower charge density is associated with the F cluster. In figure 3 we show the calculated variation in $|\mu|$ with U/B for the system described by $N = 6$, $n = \frac{5}{6}$ and $U_1 = 0$. As

expected, the magnetic moment is shown to saturate to the value $|\mu| = n$ as U/B increases. Finally, in figure 4 we show the calculated energy band structure of the system described by $N = 6$, $n = \frac{5}{6}$ and $U_1 = 0$. Since for such a system M is taken to be an integer, the Fermi energy is found, as expected, to be located in an energy gap as shown by an arrow in figure 4. Note the narrowness of the bands and the large magnitude of some gaps, in spite of the fact that the value of U/B is not so large.

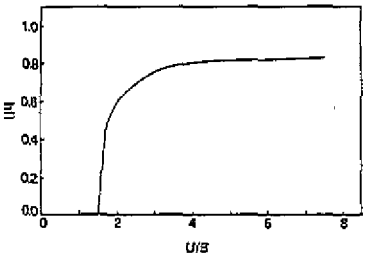

Figure 3. Variation with U/B in the mean absolute value of the magnetic moment per lattice site for a 1D periodic Hubbard system with $N = 6$, $n = \frac{5}{6}$ and $U_1 = 0$.

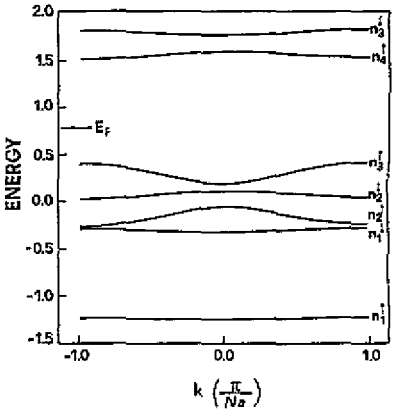

Figure 4. The lower energy bands (in units of $\frac{1}{2}B$) of up- and down-spin-electron states for a 1D periodic Hubbard system with $N = 6$, $n = \frac{5}{6}$, $U/B = 2.5$ and $U_1 = 0$. The arrow indicates the position of the Fermi level. (The nearest-neighbour distance was taken to be equal to 4.0 au.)

In order to check the effect of the size of the cluster upon the ground state of the system we have performed calculations in a system with $N = 12$ and $n = \frac{5}{6}$. For this system we have found that for values of U/B (and $U_1 = 0$) which are not so large, the ground state of the system is the one that we have found for the equivalent system with $N = 6$ and $n = \frac{5}{6}$. However, for larger values of U/B we have found that the system with the larger unit cell ($N = 12$) favours a new ground-state configuration for which in the first half of the unit cell the magnetic moments exhibit AF order while in the other half of the unit cell the magnetic moments exhibit F order. This means that, as U/B increases, the size of the local F and AF clusters increases and thus it seems that the system approaches continuously a phase-separated state, i.e. a state that results from a mixing of macroscopic domains each of which being at a particular phase chosen out of two pre-defined domains (in this example the F and AF phases). These results, although indicative of real tendencies in 2D and 3D systems, do not agree with the exact results in 1D systems.

Similar results were found for the ground state of the 1D periodic lattice with other values of n. In particular, we have studied also the cases of 1D lattices with $U_1 = 0$ and

(i) $N = 6$ and $n = \frac{4}{6}$
(ii) $N = 5$ and $n = \frac{4}{5}$
(iii) $N = 6$ and $n = 0.90$ and
(iv) $N = 6$ and $n = 0.95$.

Cases (i) and (ii) correspond to an integer M-value as in the case described previously with $N = 6$, $n = \frac{5}{6}$ and $U_1 = 0$. These three cases favour the Peierls transition and exhibit the same qualitative picture for their ground state. The other two cases, namely (iii) and (iv), do not favour the Peierls transition. Their ground state exhibits the C state found for the systems which favour the Peierls transition even for large values of U/B, being closer (than the integer M cases) to the exact results.

The stability of the C-type ground state was checked by plotting the total energy (given by equation (15)) as a function of the electron number n for various values of U/B. As shown in figure 5, the function $E = E(n)$ exhibits a clearly concave part, i.e. an indication that the system may be found in a phase-separated state between the C state on the one hand and the AF state on the other.

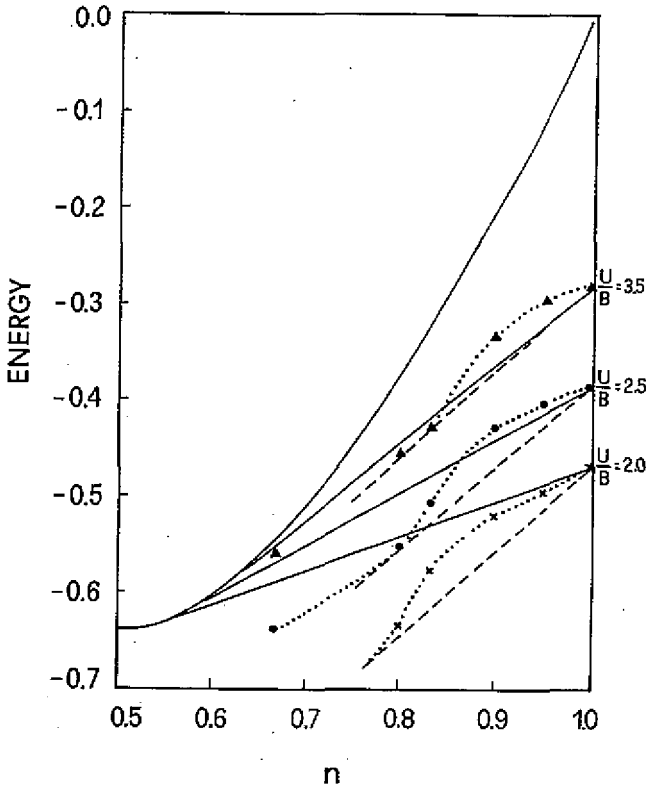

Figure 5. Energy (in units of $\frac{1}{2}B$) versus n plots for a 1D Hubbard system with $N = 6$ and $U_1 = 0$. The full curved line describes the variation in the energy of the F state. The full and broken straight lines describe the variation in the PS and PS′ states, respectively for the indicated values of U/B. The variation in the energy of the C state is indicated by the full triangles for $U/B = 3.5$, by the full circles for $U/B = 2.5$ and by the crosses for $U/B = 2.0$.

In figure 5, two families of straight lines describe the energy variation of two different phase-separated states. The full straight lines indicate the energy of a phase-separated state, denoted PS, which results from a mixing of distinctive macroscopic domains which exhibit either F or AF order. On the other hand, the broken straight lines in figure 5 indicate the energy variation of a different phase-separated state, denoted PS′, which results from a mixing of distinctive macroscopic domains which exhibit either AF order or the C state. It is worth noting that the PS′ state appears to be energetically more favoured than the PS state for $n > 0.70$ and for sufficiently low values of U/B (less than 5.0).

For each value of U/B we have compared the energy of the PS and PS′ states with the energy of the C state (obtained according to equations (5)–(15)). The various physical quantities of the system that we have calculated correspond to the lowest-energy state

including the PS and the PS′ states. Thus in figure 2 for $U/B > 4.8$ the values of δn and $\delta\mu$ have been calculated within the PS state. In the same way we have calculated the variation in $|\mu|$ with U/B shown in figure 3.

In table 1 we show the results for $|\mu|$, δn and $\delta\mu$ obtained for the ground state of systems of various n at a particular value of U/B and $U_1 = 0$. It is quite interesting to note the maximum which appears in the variation in δn and $\delta\mu$ when considered as functions of n for constant values of U/B and U_1/B.

Table 1. The average absolute value of the magnetic moment μ per lattice site and the deviations $\delta\mu$ and δn for 1D periodic Hubbard systems with the same intrasite interaction $U/B = 4.0$ and intersite interaction $U_1 = 0$ but with different average values of electrons per unit cell.

n	$\|\mu\|$	δn	$\delta\mu$
$\frac{4}{6}$	0.634	0.071	0.058
$\frac{4}{5}$	0.774	0.172	0.141
$\frac{5}{6}$	0.784	0.172	0.158
0.9	0.855	0.104	0.085

4. Phase diagram of the 1D (periodic) Hubbard model

The results for the ground state of the 1D Hubbard model found in the previous section can be compared with the results obtained within the CRFA and the conditional CPA described elsewhere [8, 13]. In figure 6 we present a diagram for the magnetic phases of the 1D Hubbard model obtained using both methods, namely the method presented in section 2 and the CRFA and the conditional CPA. As in the 3D case [13], the phase diagram of the 1D lattice exhibits the paramagnetic (P), the F, the C and the PS and PS′ regions. The PS phase consists of F and AF domains; the PS′ consists of AF and C-type domains. (The spin-glass or the spin-liquid phase of the 3D case corresponds to the C state of the 1D state.) The AF region in the 1D case was found only for $n = 1$. In figure 6 we observe that the C and PS′ states are favoured for relatively small values of U/B ($\leqslant 5.0$) the former being preferable for $0.55 \leqslant n \leqslant 0.80$ and the latter being preferable in systems with $n \geqslant 0.80$. For $U/B > 5.0$ the PS and PS′ states seem to coincide. This means that the full and the broken straight lines in figure 5 merge together within our calculation errors. For even larger U/B-values the system finally attains the F state. It must be stressed once again that the exact 1D results show a unique phase over the whole n–U plane. Thus our results are indicative of the short- and medium-range correlations that may appear in the ground state of 2D and 3D system.

The above results are in complete analogy with the recent calculations of Marder *et al* [7] who employed a MFA based on a suitable $1/N$ expansion. In particular, Marder *et al* [7] predict that for low U/B-values the ground state of the system can be a PS state, consisting of one AF domain and another exhibiting what they call the 'canted' state. Our calculated C states are in fact analogous to their 'canted' states within our Ising-model-type approximation.

To obtain an idea of what are the energy differences as one moves from one phase to another, we show in figure 7 a particular case which has $N = 6$ and $n = \frac{5}{6}$, while U/B varies.

Comparing figure 2 of [13] and the present figure 6, we see another difference between the results for the 3D case and the results for the 1D case. In the region where $U/B \to 0$

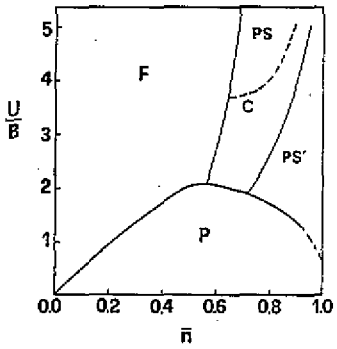

Figure 6. The phase diagram of a 1D Hubbard system obtained by firstly the CRFA and the conditional CPA as applied on a Bethe lattice of connectivity $K = 1$ and (secondly the unrestricted self-consistent MFA to the 1D periodic Hubbard system. In addition to the P and F phases, a C state appears for $0.6 \leqslant n \leqslant 0.85$ and for $2.0 \leqslant U/B \leqslant 5.0$, as well as two phase-separated states; the PS state for $U/B \geqslant 3.5$ which consists of F and AF macroscopic domains and the PS' state which appears for $U/B \leqslant 5.0$ and consists of AF and C-type domains.

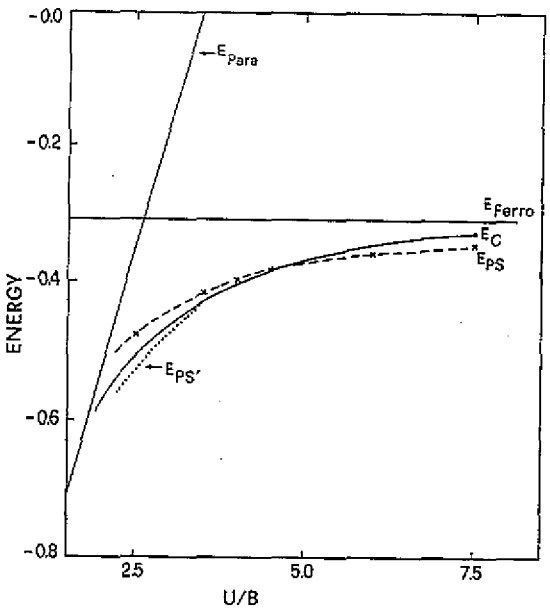

Figure 7. The energy versus U/B diagram for $n = \frac{5}{6}$ for a 1D periodic Hubbard system with $N = 6$ and $U_1 = 0$. The energy of the C, PS and PS' states are indicated by the curves labelled E_C, E_{PS} and $E_{PS'}$, respectively; the lines labelled E_{Para} and E_{Ferro} indicate the energy variation in the P and F states respectively. The energies are given in units of $\frac{1}{2}B$.

and $n \to 0$, in the 3D case the P phase always has a lower energy than all the other phases. On the other hand in the 1D case, the P phase becomes unstable when $n \to 0$ for U/B small but finite. This difference is due to the dimensionality which in the 1D case causes the DOS to be proportional to $(\delta E)^{-1/2}$, while in the 3D case it is proportional to $(\delta E)^{1/2}$ at the band edge. As a result of this, the line separating the P phase from the F phase is given by $U/B \propto n$ and $U/B \propto n^{-1/3}$ for the 1D and 3D cases, respectively. On the other hand, for $n \to 1$, both the 1D and the 3D systems exhibit the same qualitative picture as one can easily observe by comparing figure 2 of [13] and the present figure 6. This part of the phase diagram is the most interesting as this is directly related to systems of extreme practical interest, e.g. low-doped high-T_c superconductors.

5. The effect of the intersite Coulomb interactions

In this section we shall present results referring to the study of the effect of the intersite Coulomb interactions. This is achieved by allowing U_1 to be different from zero in equations

(1), (3) and (5)–(15). We restrict ourselves to the system with $N = 6$, $n = \frac{5}{6}$ and $U/B = 2.5$. In this study, U_1/B was varied from -0.7 to $+1.2$ so as to include effective attractive and repulsive interactions. For this range of the intersite Coulomb interactions the ground-state configuration was found to have the same F–AF clustering as in the case where $U_1/B = 0$. For values of $U_1/B > 1.2$ it was found that the ground state exhibits large charge fluctuations from site to site. For U_1/B in the range from -0.7 to $+1.2$ the effect of the U_1-term on the ground state is shown better in figures 8–10 where various quantities are plotted as functions of U_1/B. In particular, figures 8 and 9 show the variation in the deviations δn and $\delta\mu$, respectively, calculated according to equations (16) and (17). It is observed that δn exhibits a minimum at a non-zero value of U_1/B ($U_1/B \simeq 0.3$). In contrast, the minimum of $\delta\mu$ is found for $U_1/B = 0.0$. These results indicate that the intersite Coulomb interactions play a rather complicated and unexpected role in the development of charge and spin fluctuations. Finally figure 10 indicates the variation in the mean (absolute) value $|\mu|$ of the magnetic moment per lattice site as U_1/B changes. From this figure it is noted that, as U_1/B increases, $|\mu|$ decreases. This indicates that, as far as $|\mu|$ is concerned, increased intersite Coulomb interactions reduce effectively the role of the U/B-term. Similarly, it is observed from figure 8 that, for constant $U/B = 2.5$, an increase in U_1/B results initially in a decrease in δn. This is in fact expected from the results shown in figure 2 according to which a reduction in U/B leads to a reduction in δn and $\delta\mu$. However, as U_1/B increases, the picture changes and it is observed that a large U_1/B-term favours large fluctuations in n and μ. These observations lead us to conclude that the exact interplay between the U/B- and the U_1/B-terms needs further study in order to be established. Finally it is noted that the fluctuation $\delta\mu$ does not seem to change with small (attractive or repulsive) intersite Coulomb interactions. However, for sufficiently large U_1/B the variation in $\delta\mu$ follows that of δn.

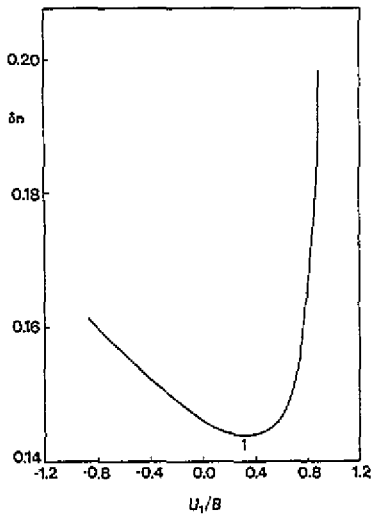

Figure 8. The deviation δn (given by equation (16)) as a function of the intersite interaction U_1/B for a 1D periodic Hubbard system with $N = 6$, $n = \frac{5}{6}$ and $U/B = 2.5$.

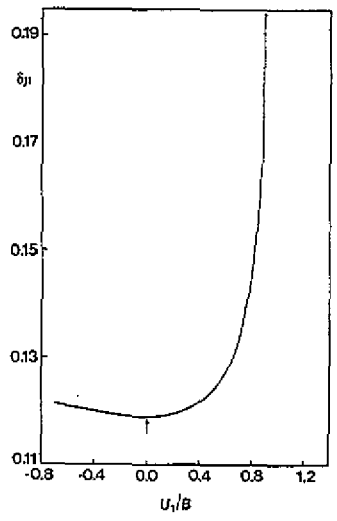

Figure 9. The deviation $\delta\mu$ (given by equation (17)) as a function of the intersite interaction U_1/B for a 1D periodic Hubbard system with $N = 6$, $n = \frac{5}{6}$ and $U/B = 2.5$.

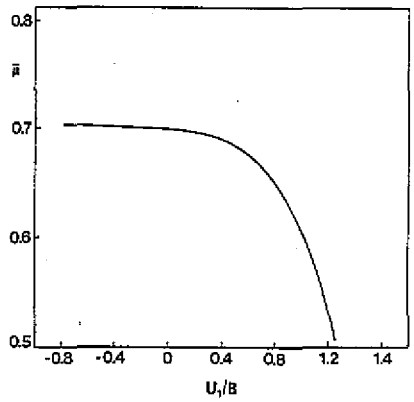

Figure 10. The average absolute value of the magnetic moment per lattice site as a function of the intersite interaction U_1/B for a 1D periodic Hubbard system with $N = 6$, $n = \frac{5}{6}$ and $U/B = 2.5$.

6. Estimation of the coupling constant J of an equivalent Ising model

Within the self-consistent MFA for the 1D Hubbard model it is possible to estimate the coupling constants J_{ij} of an equivalent Ising model. To do this we use the results for the $n_{i\sigma}$, $i = 1, \ldots, N$, for both spins σ as obtained from our self-consistent solutions. Then we reverse the spin populations of one particular site j. In other words, $n_{j\sigma}$ is taken to be $n_{j-\sigma}$ and $n_{j-\sigma}$ is taken to be $n_{j\sigma}$, i.e. we flip the local moment at j. This set of the $n_{i\sigma}$ which includes the reversed spin populations of the jth site is used as an input to equation (7). From its solution we obtain the band-structure term which contributes to the total energy given by equation (15). The change $\Delta E_b^{(j)}$ in the total energy associated with the reversal of the spin of the jth site is related to the constants $J_{j\pm1}$ of an equivalent Ising model with only nearest-neighbour couplings by the relation

$$\Delta E_b^{(j)} = 2J_{j,j-1} + 2J_{j,j+1} \tag{18}$$

with $\Delta E_b^{(j)}$ defined as (for $U_1 = 0$)

$$\Delta E_b^{(j)} = \sum_{k,\nu,\sigma}{}' E_{k\nu\sigma} - \sum_{k,\nu,\sigma} E_{k\nu\sigma} \tag{19}$$

where the prime indicates that the summation refers to the system with one spin flipped over at site j.

We proceed next by calculating $\Delta E^{(j+1)}$ which is

$$\Delta E_b^{(j+1)} = 2J_{j+1,j} + 2J_{j+1,j+2}. \tag{20}$$

Then we find the energy change $\Delta E_b^{(j,j+1)}$ associated with the reversal of the spins at sites j and $j+1$:

$$\Delta E_b^{(j,j+1)} = 2J_{j-1,j} + 2J_{j+2,j+1}. \tag{21}$$

From equations (18), (20) and (21) we have

$$\tfrac{1}{4}(\Delta E_b^{(j)} + \Delta E_b^{(j+1)} - \Delta E_b^{(j,j+1)}) = J_{j,j+1}. \tag{22}$$

Table 2. Calculated coupling constants J_{ij} (in units of $\frac{1}{2}B$) of a 1D periodic Hubbard system described by $N = 6$, $n = \frac{5}{6}$, $U_1 = 0$ and $U/B = 2.5$. The small negative values indicate instability of the ground state.

J_{12}	J_{23}	J_{34}	J_{45}	J_{56}	J_{61}
0.0236	−0.0040	0.0263	0.0112	0.0387	−0.0013

The determination of one $J_{j,j+1}$ allows us to find all the others if the energy changes $\Delta E_b^{(j)}$, $j = 1, \ldots, N$ are known.

In table 2 we present the results of the J_{ij}-values for a system with $N = 6$, $n = \frac{5}{6}$, $U_1 = 0$ and $U/B = 2.5$ obtained according to equations (18)–(22).

The validity of equation (22) relies on the basic assumption that the reversal of one spin affects only the bonds of the nearest neighbours. Such an assumption can be easily checked within the present scheme as follows. We calculate the coupling constants J_{ij} starting from two different pairs $(j, j+1)$ and compare the two sets of the constants J_{ij} which are obtained. Such a comparison has been done and has shown that, at least for some values of the parameters, the assumption used to derive equation (22) is not valid and one has to include interactions between second-nearest neighbours. Thus the values given in table 2 do not describe accurately the magnetic couplings in the system.

On the other hand, the calculation of J-values allowed us to check the stability of the ground-state configurations described in section 3 and helped us to determine the ground-state configuration with the lowest energy for a given set of the parameters of the system. In other words we have observed that a negative or very small $\Delta E_b^{(j)}$-value indicates that the process of spin flipping which we had allowed the system to undergo leads to a stabler ground-state configuration compared with the configuration that we had started with. Thus the spin-flipping process could lead us to the determination of an energetically more favoured configuration, a procedure that we follow in our calculations. Furthermore, the coexistence of large J_{ij} as well as small (almost zero) J_{ij} indicate that our cluster state is a mixture of spin-glass as well as spin-liquid character. Finally negative or very small J-values are indicative that the MFA is becoming unreliable. This is important because it shows that our MFA provides clear signs where its limits of validity are approached.

7. Conclusions

In the present work we studied the effects of spin and charge correlations as well as the effects of spin and charge fluctuations on the ground state of the Hubbard model by employing an unrestricted self-consistent MFA to the 1D periodic Hubbard model. It was found that for a certain range of the values of the parameters of the system the ground state of the Hubbard model favours cluster formation consisting of higher-charge 'AF' domains and lower-charge F regions. For a certain range of values of our parameters the clusters become larger and larger and eventually drives the system to full phase separation. In the phase-separated state, the system consists of macroscopic domains which exhibit a well defined phase. According to our findings a phase-separated state (denoted by PS) was found to consist of F and AF domains and to be favoured in systems with large values of U/B. Another phase-separated state (denoted by PS′) was found in systems of relatively low U/B-values and was found to consist of domains which exhibit the AF or the C state. The main characteristic of the C state is that at this state the tendency for phase separation is developed locally within a microscopic region. In one part of this region the electrons exhibit F order

while in the rest of the region the electrons exhibit AF order. For certain values of the number of electrons per lattice site, it was found that, as U increases, the F cluster of the local phase-separated state increases at the expense of the AF cluster. For further increase in U the system attains either directly the F phase or passes firstly through a phase-separated state before it becomes a ferromagnet. It was also found that this picture does not change substantially either with the size of the artificial unit supercell or with small moderate changes in the value of the intersite (nearest-neighbour) repulsive or attractive interactions.

The model cases that we studied included systems with unit supercells having $N \leqslant 12$. Analysing our results we observed that by increasing N, i.e. by considering systems with larger unit cells, we find an increasing number of lowest-lying states that exhibit spin configurations which differ very little in energy from each other. This observation makes clear that, as N increases, it will become prohibitively expensive, if possible at all, to obtain computationally a unique ground-state configuration of the system. This problem was found to become more and more pronounced as U/B increases. Similar findings were recently reported for the 2D systems by Inui and Littlewood [18].

It must be pointed out that our method, although quite sophisticated, omits quantum fluctuations which may drive the system to different ground states. This was shown by recent theoretical and numerical investigations [15–17] on the exact spin–spin correlations of the 1D Hubbard and the t–J models which indicated that for such systems the ground state is of a short-range AF nature. The picture that emerges from these exact 1D considerations indicates the effect of neglecting quantum fluctuations and the limitations of the MFA which adopt such an approximation. However, in systems of higher dimensionality (2D and 3D systems), one might expect the effect of quantum fluctuations not to be strong enough (as in the 1D case) to overcome the short-range order clustering effects and therefore this may allow the system to attain a PS′ ground state.

Having clarified that our unrestricted Hartree results are more relevant for the 2D or 3D cases than for the 1D case for which they were obtained, we discuss now their relevance to high-T_c superconductivity. The existence of appreciable values of charge fluctuation δn allows the possibility, when quantum fluctuations are taken into account, of a superconducting state. Indeed, quantum fluctuations either may stabilize the system to a charge-density state (as the mean field shows) or may drive it to a superconducting state if the charge fluctuations move through the system in a correlated way. In fact, in the 2D case, local clusters of charges can easily move around collectively, indicating that the possibility of superconductivity is favoured in higher dimensionality. On the basis of our results, superconductivity may appear for relatively large values of U/B (larger than 1.5) and values of n close to unity (in order to prevent an easy spin-flip scattering of the electron pair by the local moments, which for n close to unity exhibit strong AF coupling). Note that a relatively large intersite repulsive interaction may further enhance the possiblity of superconductivity. It is worthwhile to note that our calculation indicates a rather strong indirect hole–hole attraction; we estimated this effective attraction by finding the value of an *attractive* on-site U, which will give us the same value of δn. We found a surprisingly strong $U/B \simeq -2$, more than enough to provide strong hole–hole binding.

Regarding the question of phase separation we expect that long-range Coulomb forces will prevent its occurrence, unless one assumes macroscopic or mesoscopic inhomogeneities in the specimen which are related to variations in the local concentration of oxygen. However, microscopic clusters of the type found in the C state are expected to survive the long-range Coulomb forces. It is worth pointing out that the C state has characteristics of a spin-glass and spin-liquid phase (the former is associated with regions of relatively high magnetic couplings while the latter with very small (or even negative) J-values). In

view of this, a marginal Fermi liquid behaviour cannot be considered as inconsistent with our findings.

Finally, we point out that our calculations strongly indicate that, if a superconducting state will be established, it will coexist with strong AF magnetic order.

Acknowledgments

This work was partially supported by EEC research grant (Esprit-3041), the Commission of the European Communities through grant SCC* CT90-0020 and the NATO travel grant RG769/87. The work of CMS was also supported by the US Department of Energy grant W-74O5-ENG-82. We thank N Papanicolaou and G Psaltakis for valuable discussions.

References

[1] Hubbard J 1963 *Proc. R. Soc.* A **276** 236
[2] Zhang F C and Rice T M 1988 *Phys. Rev.* B **37** 3756
[3] Anderson P W 1987 *Science* **235** 1196; 1988 *Frontiers and Borderlines in Many Particle Physics (Proc. Enrico Fermi Int. Summer School of Physics 104) (Varenna (1987)* ed R A Broglia and J R Schneffer (Amsterdam: North-Holland) p 1 and references therein
[4] White S R, Scapalino D J, Sugar R L, Loh E Y, Gubernatis J E and Scalettar R T 1989 *Phys. Rev.* B **40** 506
Hirch J E and Tang S 1989 *Phys. Rev. Lett.* **62** 591
[5] Sorella S, Car R, Baroni S and Parrinello M 1989 *Europhys. Lett.* **8** 663
Sorella S, Parola A, Parrinello M and Tosotti E 1989 *Int. J. Mod. Phys.* B **3** 1875
Parola A, Sorella S, Boroni S, Parrinello M and Tosotti E 1989 *Int. J. Mod. Phys.* B **3** 1865
[6] Callaway J, Chen D P, Kanhere D G and Qiming Li 1990 *Phys. Rev.* B **42** 465
[7] Marder M, Papanicolaou N and Psaltakis G C 1990 *Phys. Rev.* B **40** 6920
Emery V J, Kirelson S A and Lin Q 1990 *Phys. Rev. Lett.* **64** 475
[8] Andriotis A N, Qiming Li, Economou E N and Soukoulis C M 1991 *Dynamics of Magnetic Fluctuations in High-Temperature Superconductors* ed G Reiter, P Horsch and G C Psaltakis (New York: Plenum) p 267
[9] Economou E N, White C T and DeMarco R R 1978 *Phys. Rev.* B **18** 3946
White C T and Economou E N 1978 *Phys. Rev.* B **18** 3959
DeMarco R R, Economou E N and White C T 1978 *Phys. Rev.* B **18** 3968
Economou E N and Mihas P 1977 *J. Phys. C: Solid State Phys.* **10** 5017
Economou E N and White C T 1977 *Phys. Rev. Lett.* **38** 289
[10] Liu S H 1978 *Phys. Rev.* B **17** 3629
[11] Andriotis A N, Poulopoulos P N and Economou E N 1981 *Solid State Commun.* **39** 1175
[12] Economou E N 1983 *Green's Functions in Quantum Physics* (Berlin: Springer)
[13] Andriotis A N, Economou E N, Li Q and Soukoulis C M 1993 *Phys. Rev.* B (in press)
[14] Lieb E H and Wu F Y 1968 *Phys. Rev. Lett.* **20** 1445
[15] Ogata M, Luchini M U, Sorella S and Assaad F F 1991 *Phys. Rev. Lett.* **66** 2388
[16] Schulz H J 1990 *Phys. Rev. Lett.* **64** 2831
[17] Parola A and Sorella S 1990 *Phys. Rev. Lett.* **64** 1831
[18] Inui M and Littlewood P B 1991 *Phys. Rev.* B **44** 4415